S.N. Gerasimov, P. Abreu, L.R. Baylor, A. Boboc, I.S. Carvalho, I.H. Coffey, D. Craven, V. Huber, S. Jachmich, E. Joffrin, U. Kruezi, M. Lehnen, P.J. Lomas, A. Manzanares, M. Maslov, E. Matveeva, G. Pautasso, A. Peacock, S. Silburn, C. Stuart, H. Sun, D. Shiraki, R. Sweeney, J. Wilson, L.E. Zakharov

Mitigation of disruption electro-magnetic load with SPI on JET-ILW

Mitigation of disruption electro-magnetic load with SPI on JET-ILW

S.N. Gerasimov, P. Abreu, L.R. Baylor, A. Boboc, I.S. Carvalho, I.H. Coffey, D. Craven, V. Huber, S. Jachmich, E. Joffrin, U. Kruezi, M. Lehnen, P.J. Lomas, A. Manzanares, M. Maslov, E. Matveeva, G. Pautasso, A. Peacock, S. Silburn, C. Stuart, H. Sun, D. Shiraki, R. Sweeney, J. Wilson, L.E. Zakharov

Mitigation of disruption electro-magnetic load with SPI on JET-ILW

S.N. Gerasimov[1], P. Abreu[2], Yu.F. Baranov[1], L.R. Baylor[3], A. Boboc[1], I.S. Carvalho[2], I.H. Coffey[1,4], D. Craven[1], V. Huber[5], S. Jachmich[6], E. Joffrin[7], S.I. Krasheninnikov[8], U. Kruezi[6], M. Lehnen[6], P.J. Lomas[1], A. Manzanares[9], M. Maslov[1], E. Matveeva[10,11], G. Pautasso[12], A. Peacock[1], S. Silburn[1], R.D. Smirnov[8], C. Stuart[1], H. Sun[1], D. Shiraki[3], R. Sweeney[13], J. Wilson[1], L.E. Zakharov[14,15] and JET Contributors[a]

EUROfusion Consortium, JET, Culham Science Centre, Abingdon, OX14 3DB, UK

[1] *UKAEA/CCFE, Culham Science Centre, Abingdon, Oxon, OX14 3DB, UK*
[2] *IPFN, Instituto Superior Técnico, Universidade de Lisboa, Lisboa, Portugal*
[3] *Oak Ridge National Laboratory, Oak Ridge, TN 37831, United States of America*
[4] *Astrophysics Research Centre, Queen's University, Belfast, BT7 1NN, UK*
[5] *Jülich Supercomputing Centre, Forschungszentrum Jülich, 52425 Jülich, Germany*
[6] *ITER Organization, Route de Vinon, CS 90 046, 13067 Saint Paul Lez Durance, France*
[7] *CEA, IRFM, F-13108 Saint-Paul-lez-Durance, France*
[8] *University of California San Diego, La Jolla, CA 92093, United States of America*
[9] *Laboratorio Nacional de Fusión, CIEMAT, 28040 Madrid, Spain*
[10] *Charles University, Faculty of Mathematics and Physics, Prague, Czech Republic*
[11] *Institute of Plasma Physics of the CAS, Prague, Czech Republic*
[12] *Max-Plank-Institute für Plasma Physik, D-85748 Garching, Germany*
[13] *MIT Plasma Science and Fusion Centre, Cambridge, MA 02139, United States of America*
[14] *LiWFusion P.O. Box 2391, Princeton NJ 08543, United States of America*
[15] *Department of Physics, University of Helsinki, P.O. Box 43, FIN - 00014, Finland*
[a] *See 'Overview of JET results for optimizing ITER operation' by J. Mailloux et al, to be published in Nucl. Fus. Special Issue for 28th Fusion Energy Conference (2021)*
E-mail: *Sergei.Gerasimov@ukaea.uk*

Introduction. The disruption mitigation system design for ITER consists of shattered pellet injectors (SPI) that can inject up to 27 pellets (24 from three equatorial ports and 3 from upper ports), which will be dedicated to the mitigation of electro-magnetic loads (EML), thermal loads, and the avoidance and suppression of runaway electrons [1]. Recently the JET-ILW was equipped with an SPI with a wide capability [2][3]. Specifically: pellet diameter d = [4.57, 8.1, 12.5] mm (which were referred to here as pellet C, B and A, respectively) and effective length/d ratio = [1.4, 1.6, 1.54]; pellet compositions of D_2, Ne with D_2 shell, D_2+Ne mixture, and Ar. The pellets are fired by high pressure propellant gas or a gas operated mechanical punch to release the pellets. The fully commissioned system became operational in July 2019.

Diagnostics. The SPI experiment essential diagnostics include (1) Barrel Valve Current, (2) Microwave cavity (MWC), (3) AXUV Diamond Detector which records radiation E > 5.5 eV
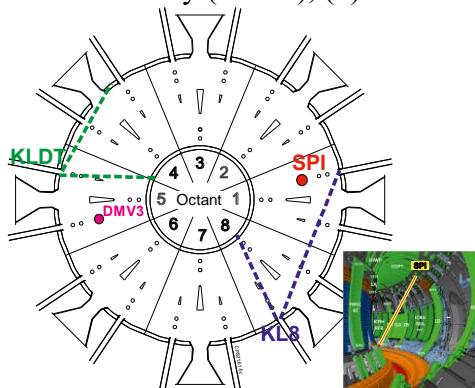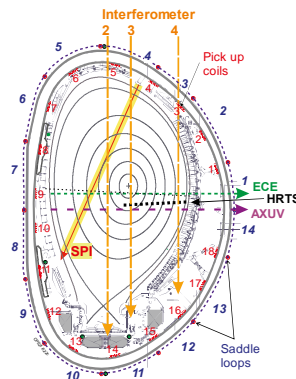

Fig. 1 SPI, Fast Visible Cameras and DMV3.

Fig. 2 Essential diagnostics.

(λ < 226 nm), (3) Fast Visible Cameras KL8 and KLDT with (10-20) kHz rate, (33.3-50) μs frame while KL8 can be equipped by filters to see Ne I atoms (692.8 nm) or Ar I atoms or Ar II ions (611.6 nm), (4) Electron Cyclotron Emission (ECE), (5) High Resolution Thomson

Scattering (HRTS), (6) Interferometer with 195 μm and 119 μm beams, (7) Magnetics, Fig. 1 and Fig. 2.

The pellets pass through the MWC, and the number of peaks in the MWC signal reliably indicates the number of intact/broken pellet pieces, Fig. 3a. The amplitude of the MWC does not solely depend on the mass of the pellet. The dielectric constants for solid D_2, Ne and Ar are different and that is what changes the Q-factor of the cavity and determines the magnitude of the signal. If the pellets were all D_2 then the magnitude would be proportional to the D_2 mass. The pellets A and pellets B give good amplitude signals whilst pellets C produce a signal with a small amplitude, Fig. 3b.
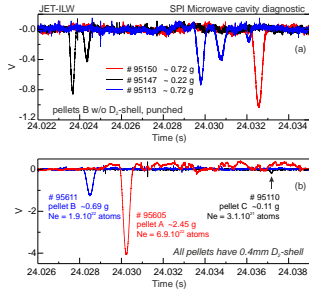

Fig. 3 MWC indicates (a) the number of intact/broken pellet pieces, (b) for given substance the MWC amplitude proportional to pellet mass.
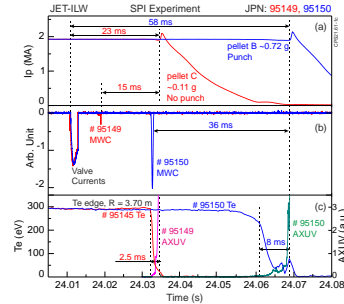

Fig. 4 The pellets instigate disruption: (a) plasma currents, (b) valve current and MWC signal, (c) Te at the plasma edge and AXUV light.

Pellet ablation and assimilation. The experiment was performed with ohmic plasma with I_p = 1.1-2.9 MA, average line density $n_e l \approx 2 \cdot 10^{19}$ m^{-2}, which corresponds to total number of plasma electrons $n_e \cdot V \approx 6 \cdot 10^{20}$ and mainly pellets with D_2 shell and D_2+Ne composition. The typical time needed for pellet to instigate a disruption is ~ 20 ms for small pellet C (#95149, ~ 0.11 g, Ne/(Ne+D) = 0.60, Ne = 3.07 $\cdot 10^{21}$ atoms) fired by gas and ~ 60 ms for medium pellet B (#95150, ~ 0.72 g, Ne/(Ne+D) = 0.64, Ne = 2.04 $\cdot 10^{22}$ atoms) fired by mechanical punch, Fig. 4. Thus, the pellets fired without the use of a punch are faster than punched pellets. The speed of the pellet is calculated from the time of flight between the MWC and either AXUV or, better, the start of the rise in fast camera Ne I total intensity. The estimated speed of the pellet C (#95149) is ~ 380 m/s and pellet B (#95150) is ~140 m/s, Fig. 4.

The pellets cause cooling of the plasma periphery, then Thermal Quench (TQ) followed by Current Quench (CQ).

The small pellet C (#95149) lead to a cooling phase duration ~ 2.5 ms and TQ duration ~ 0.5 ms, Fig. 5. The Te degrades at the plasma edge during the cooling phase, namely Te drops almost to zero in the external plasma region of ~1/3 minor radii, then the centre Te drops during TQ, Fig. 6. The first results of modelling of #95149 disruptions using M3D-C1 presented in the [4]. Neutral Ne I line image is not visible during the main time of the CQ, hence the small pellet C is ablated and presumably assimilated during cooling, TQ and MHD phases.

For similar plasma, the interaction of medium pellet B with plasma is significantly different: neutral Ne I line image is visible during by the end of the CQ, Fig. 7. Therefore, the Ne neutrals exist even at the end of CQ. Thus, the pellet is not fully ablated, and therefore clearly not fully

assimilated, by the end of the CQ. Consequently, medium B (and presumable large A) pellets are unnecessarily big to mitigate Ohmic plasmas with $I_p < 3$ MA.
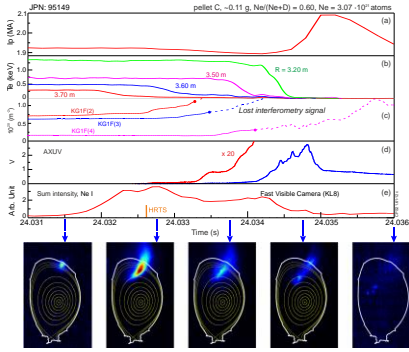

Fig. 5 Small pellet C instigates disruption: (a) plasma current, (b) electron temperature, (c) line density, (d) light,(e) Ne I intensity.
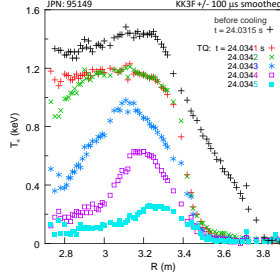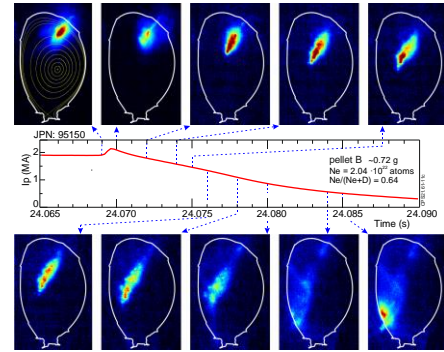

Fig. 6 Te profiles during TQ phase.

Fig. 7 Medium pellet B instigates disruption but is not fully assimilated by the end of the CQ.

Effect pellet parameters on CQ duration. The CQ time duration, τ_{80-20}, is the key characteristic of mitigation effectiveness. This study reveals: (a) strong dependence of τ_{80-20} on Ne (or Ar) fraction, Fig. 8; (b) τ_{80-20} does not depend on number of Ne atoms (in other words pellet size) for Ne/(Ne+D) > 0.5, however, it is easy to make the opposite incorrect conclusion, if the whole
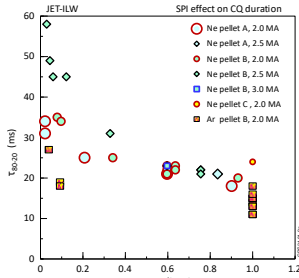

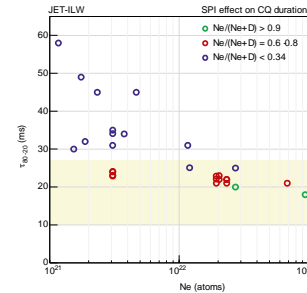*Fig. 8 Strong dependence of CQ duration on Ne (Ar) fraction.*

Fig. 9 CQ duration dependence on number of Ne atoms in a pellet. The desirable JET τ_{80-20} is shown by shaded yellow area [5].

range of the Ne fraction is considered, Fig. 9; (c) a marginal effect of pellet integrity and pellet size on τ_{80-20}; (d) SPI efficacy, in terms of τ_{80-20}, does not depend on pre-disruptive I_P (in another words on the poloidal magnetic energy) for $I_p < 3.0$ MA and middle-sized pellets.

Effectiveness of SPI on post-disruptive plasma. The disruption mitigation is meant to be applied on off-normal or post-disruptive plasmas. In presented experiments, the SPI was applied
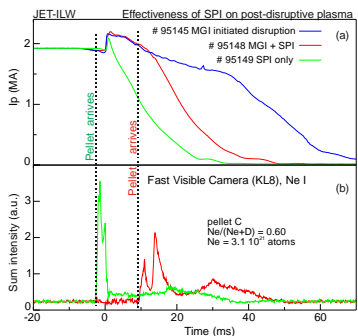

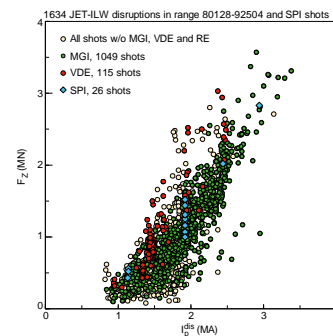*Fig. 10 Effectiveness of SPI on post-disruptive plasma: (a) plasma current, (b) Ne I intensity.*

Fig. 11 Effectiveness of SPI on axisymmetric forces.

mainly on normal ("healthy") plasma i.e., not prone to disruption plasmas. However, the effect on post-disruptive plasma has also been tested, by using Massive Gas Injection (MGI) to instigate

disruptions, Fig. 10. Then this MGI instigated disruption #95145 pulse is used as a reference pulse for SPI mitigation of post-disruptive plasma, pulses #95148. This study shows that SPI effectiveness (in terms of τ_{80-20}) does not depend on plasma status, see #95149 ("healthy" plasma) and #95148 (post-disruptive plasma), Fig. 10. So cooling and TQ phases are not essential for CQ duration.

Effectiveness of SPI on Axisymmetric Forces AVDE. SPI reduced the axisymmetric vertical vessel reaction forces relative to unmitigated disruptions, Fig. 11. Effectiveness is comparable with MGI [5]. Vessel reaction vertical forces for SPI (and MGI) mitigated disruptions are below non-mitigated VDEs and below the upper bound of non-mitigated disruptions.

Pellet arrival stopped vertical movement of plasma, Fig. 12. Comparison is made with a late pellet arrival (#95110), where pellet did not enter plasma and correspondingly did not eliminate vertical plasma displacement. One of the results of the experiment was prevention of Asymmetrical Vertical
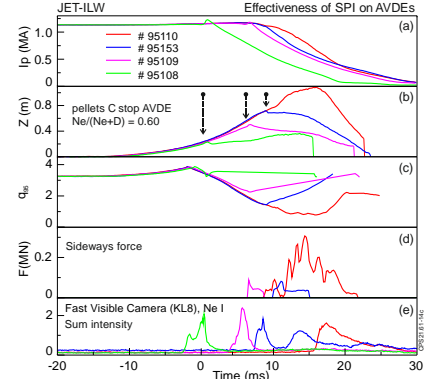

Fig. 12 Pellet arrival stopped vertical movement of plasma: (a) plasma current, (b) vertical plasma displacement, (c) safety factor, (d) Noll's sideways force, (e) Ne I intensity. The time axis is zeroed to Tdis.

Displacement Events (AVDEs) by SPI, namely the safety factor q_{95} increases (or stays the same) and, presumably, eliminates the excitation of the $m=1$, $n=1$ kink mode, responsible for AVDE. In this regard, the effect of SPI is similar to the effect of MGI [5].

SUMMARY

Small (0.1 g) pellet C with Ne/(Ne+D) = 0.6 provides good mitigation for I_p < 2 MA Ohmic plasmas. Pellets B are not fully ablated and assimilated by the end of CQ, therefore medium pellet B (and large pellet A) are unnecessarily big to mitigate Ohmic plasmas with I_p < 3 MA. There is a strong dependence of CQ duration on Ne fraction. SPI effectiveness (in terms of τ_{80-20}) does not depend on pre-disruptive I_p (< 3.0 MA, pellet B). CQ duration does not depend on #Ne atoms (= pellet size) for Ne/(Ne+D) > 0.5. SPI effectiveness (in terms of τ_{80-20}) does not depend on plasma status: it is effective in normal ("healthy") plasma i.e. not prone to disruption as well as post-disruptive plasma. SPI reduced vertical vessel reaction forces relative to unmitigated disruptions. Effectiveness is comparable with MGI. Pellet C (60% Ne) arrival stopped vertical movement of plasma, hence SPI prevents AVDE, when large vessel asymmetric (radial) displacement occurs.

Reference

[1] M. Lehnen *et al.*, "The ITER Disruption Mitigation Strategy," *Tech. Meet. Pl. Disruptions their Mitig.*, 2020.

[2] S. Jachmich *et al.*, "Shattered pellet injection experiments at JET in support of the ITER disruption mitigation system design," *FEC 2020, EX/5-1Ra*, 2021.

[3] L. R. Baylor *et al.*, "Design and performance of shattered pellet injection systems for JET and KSTAR disruption mitigation research in support of ITER," *FEC 2020, TECH/1-4Rb*, 2021.

[4] O. P. Bardsley *et al.*, "Extended-MHD simulations of shattered pellet injection into an Ohmic JET plasma," *this conf., poster*

[5] S. N. Gerasimov *et al.*, "Overview of disruptions with JET-ILW," *Nucl. Fusion*, vol. 60, no. 6, 2020.